Materials Research Proceedings 54 (2025) 159-169 https://doi.org/10.21741/9781644903599-18

Microstructural and defects investigation of AlCrFeMnNi-based high entropy alloy fabricated via laser powder bed fusion

Abdul Herrim Seidou[1,a *], Catherine Blondiau[1,b], Olivier Dedry[1,c], Jérôme Tchoufang Tchuindjang[1,d], and Anne Mertens[1,e]

[1] Metallic Materials Science (MMS), A&M Dpt., University of Liège, Liège, 4000, Belgium.

[a]ahb.seidou@uliege.be, [b]catherine.blondiau@student.uliege.be, [c]olivier.dedry@uliege.be, [d]j.tchuindjang@uliege.be, [e]anne.mertens@uliege.be

Keywords: Additive Manufacturing, Laser Powder Bed Fusion, High Entropy Alloys, Defects, Microstructure

Abstract. $Al_{0.15}CrFe_{2.9}Mn_{1.7}Ni_{2.1}Mo_{0.2}$ high entropy alloy (HEA) powder's mixture was prepared manually by blending 316L stainless steel with elemental powders. The mixture was processed through Laser Powder Bed Fusion (LPBF) to achieve a face-centered cubic (FCC) structure, aiming to enhance corrosion resistance. Since the powders used were not designed for LPBF, this study investigates the effects of powder characteristics and scanning strategies on the resulting microstructure with a focus on the defects assessment. After optimizing the processing parameter window through single tracks printing, the scanning strategy is selected while varying laser power, scanning speed and remelting step. Microstructure analysis of the printed samples was conducted by combining Optical Microscopy (OM) and Scanning Electron Microscopy (SEM). The analysis revealed the presence of hot cracks and unmelted agglomerates of refractory elements, and other compositional heterogeneities in all the samples. The findings provide a basis for developing optimized printing strategies and producing defects-free printed samples.

Introduction

Laser Powder Bed Fusion (LPBF), an Additive Manufacturing (AM), enables the production of complex geometries and features that are challenging for conventional methods. LPBF has revolutionized the manufacturing of components previously fabricated through techniques such as injection molding or die-casting, offering design flexibility and material efficiency. The fabrication process generates high cooling rates in comparison to conventional techniques [1].

LPBF involves several physical phenomena such as reflection or absorption of the laser beam, phase transformations, heat transfer, solidification, chemical reactions, and the flow of molten metal in the melt pool (MP). The MP may form due to the conversion of laser energy into heat, adopting the shape of a circular or segmented cylinder due to the surface tension [2]. The step thermal gradients within the MP lead to intricate hydrodynamic flows such as Marangoni convection, which can cause spatter formation. These spatters can disrupt the powder bed homogeneity, generating defects such as irregularities and incomplete layer fusion in subsequent tracks [3]. In recent years, many studies investigated the influence of process parameters on the quality of the final parts [4,5].

In powder bed fusion processes, powder morphology, especially particle shape, and powder size distribution, will affect laser absorption, powder bed density and thermal conductivity that finally set the quality of the printed parts. Finer particles should provide greater surface area and more efficiently absorb laser energy than coarser particles [2].

In recent years, in-situ alloying from blended powders emerged as a new approach to explore novel alloy compositions for LPBF. This method consists in mixing either elemental or pre-alloyed powders, or a combination of both, to achieve targeted compositions. However, achieving

chemical homogeneity of the printed part remains a great challenge when using this approach. A larger MP will involve more powder, thus increasing the volume of powder to be melted. As a result, a better approximation of the overall composition of the powder's mixture will be obtained. Although guidance on optimal remelting routes is still lacking, printing strategies such as remelting steps have been shown to improve the homogeneity of local chemistries within parts built from mixed powders [6].

Improper scanning parameters and inadequate powder melting can lead to porosities, poor surface finish, balling, residual stresses, and many other defects associated with unstable MP, which can deteriorate the properties and impede large-scale industrial adoption [3]. Additionally, the scanning strategy impacts macrostructure that is set as crystals grow epitaxially, as columnar dendrites, or as cellular structure, thus yielding complex shrinkage stress. Residual stresses occurring during the solidification stage within parts made by LPBF process contribute to the initiation of hot cracks. Moreover, reactions of precipitation and/or the formation of a liquid film during solidification (that is affected by alloying elements, freezing range and solidification rate), can also cause cracking [7].

High entropy alloys (HEAs), originally defined as alloys that contain more than five elements with equiatomic compositions between 5% and 35%, have lately been extended to alloys with only four main elements [8,9]. HEAs exhibit exceptional properties due to their high mixing entropy effect, typically forming body-centered cubic (BCC) or face-centered cubic (FCC) lattice structures. BCC HEAs offer high strength but low ductility, while FCC HEAs are characterized by high ductility and improved wear and corrosion resistances [10]. The high cooling rates achieved under LPBF process can reduce or suppress compositional segregation and intermetallics formation in the printed part, enhancing the mechanical properties through grain refinement and solid solution strengthening [11].

The microstructure of HEAs that is influenced by both the alloying elements and the scanning strategies, plays a crucial role in determining properties such as corrosion resistance. Elements like Al and Cr affect corrosion behavior. In alloys with high Al content, a porous oxide film will develop on the surface, which will fail to effectively protect against Cl^- permeation. In addition, Al will promote BCC phase within the bulk, which will exhibit inferior corrosion behavior compared to FCC. The depletion in Cr inside the BCC phase will also lead to elemental segregation. Therefore, a control of the microstructure in developing materials with targeted properties requires a comprehensive understanding of the effects of scanning strategies and the role of alloying elements [12].

This study aims to investigate the effects of powders mixing and of scanning strategies on the one hand, and of the alloying elements on the other hand, on defects occurrence within HEAs processed by LPBF. Such a work will enable to address challenges that arise from compositional heterogeneities and raw material impurities.

Methods

Elemental powders supplied by Abcr GmbH (Germany) were mixed with commercial gas atomized 316L Stainless Steel (SS) to reach the composition of $Al_{0.15}CrFe_{2.9}Mn_{1.7}Ni_{2.1}Mo_{0.2}$. The nominal composition of the powder is outlined in Table 1. Among all the powders used to prepare the mixture, only 316L SS and Mn elemental powder had spherical shape and a size distribution around 45 μm, which is well suited for LPBF processing.

Table 1 – Nominal composition of 316L SS.

wt. %	C	Cr	Ni	Mo	Mn	Si	Fe
316L SS	0.03	18	14	3	2	1	Bal.

20 cubes numbered from 1 to 20, with 10x10x10 mm³ sizes, were produced using an Aconity MINI LPBF printer under Argon atmosphere. Several values of laser powers (P) and scan velocities (v_s) were used, as shown in Table 2. Those parameters were selected by performing single track experiments in a wider range of P and v_s. The tracks were analysed under an optical microscope to identify and to exclude the parameters showing a strong instability of the melting regime and a poor melting of powder bed. This methodology is well known for the development of optimal process parameters [13]. A laser spot of 80 µm with a gaussian distribution, a layer thickness (t) of 30 µm and a hatch spacing (h) of 90 µm were used for all samples. The scanning strategy was set as a 90° rotation for each layer, without contouring. A preheating of 200°C was used during the printing process. Samples 16 to 20 were printed using a remelting step. Each layer is remelted with the same experimental parameters and scan strategy. A good dimensional accuracy is reached for all the samples, according to the initial geometrical features. The volumetric energy density (Ed) was calculated based on the processing parameters (Eq. 1).

$$Ed = \frac{P}{t * h * v_s} \quad (1)$$

Table 2 – Printing parameters of Al0.15CrFe2.9Mn1.7Ni2.1Mo0.2 powder's mixture.

Samples	P [W]	v_s[mm/s]	Ed [J/mm³]
1	150	400	139
2	150	600	93
3	150	800	69
4	150	1000	56
5	175	400	162
6	175	600	108
7	175	800	81
8	175	1000	65
9	185	600	114
10	185	800	86
11	185	1000	69
12	185	1200	57
13	200	600	123
14	200	800	93
15	200	1000	74
16=3 with remelting	150	800	69
17=7 with remelting	175	800	81
18=10 with remelting	185	800	86
19=14 with remelting	200	800	93
20=15 with remelting	200	1000	74

The surface of the as-built samples was checked using an Alicona Infinite Focus G5 optical profilometer for roughness analysis. All the as-built samples were cut by Electro Discharge Machining perpendicularly to the laser scan direction of the last layer, to obtain the vertical cross section. After cutting, samples were hot mounted with an electrically conductive resin, then ground and polished down to 1 µm. Samples were etched with 3% Nital to reveal specific microstructural features. Defects within the cross sections were analysed through an optical microscope Olympus BX60 and a scanning electron microscope (SEM) Tescan Clara Ultra-High Resolution UHR.

Results and Discussion

General Overview. Samples 1 and 5, showing evident surface defects that compromised layer quality, were excluded from further investigation. Since all the powders used to prepare the mixture were not well suited for LPBF process, the study focused on investigating the effects of the elemental powders and of the scanning strategy on the microstructure. Notably, none of the samples were completely defects-free, as will be discussed in the following sections.

Among the samples evaluated, samples 1 and 5 exhibit the lowest relative density, i.e. around 96.3%. Samples 3 and 17, on the other hand, were specifically selected for deeper analysis due to their highest relative density (>98%) and their good surface finish, as determined through roughness analysis. These two samples also represent distinct remelting strategies and share a medium-low energy density, as shown in Table 2.

As observed in Fig. 1, samples 3 and 17 present hot cracks in the microstructure, mostly oriented along the building direction. This observation from samples provides insights into the MP behavior. The melting strategy influences the appearance of the MP. Significant shape fluctuations in the MP can be observed in sample 3 after complete solidification (Fig. 1a). Such a result is consistent with Wang et al. [3] and is due to the compositional heterogeneity to be discussed later. Conversely, in sample 17, which underwent one remelting of each layer using the same scanning parameters, no fluctuations occur within the MP (Fig. 1b). In both samples, unmelted Mo agglomerates were observed (Fig. 1b). Those agglomerates were formed during blending of the powders which did not ensure a perfectly homogeneous mixture.

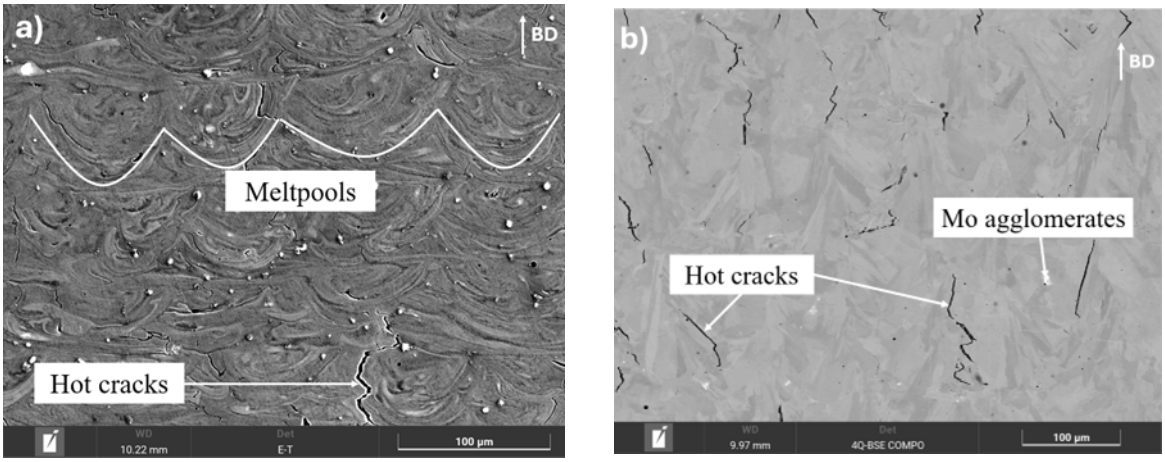

Figure 1 – SEM micrographs (after Nital etching): (a) Fluctuations within MP, Mo agglomerates, and hot cracks in Sample 3, (b) Hots cracks and elemental agglomerates in Sample 17.

The following sections examine the challenges associated with mixing several powders, particularly when some powders are not well suited for the LPBF technology.

First, issues related to the (incomplete) dissolution of refractory elements will be reviewed, followed by a broader investigation into chemical heterogeneities. Finally, the various factors affecting hot crack formation will be discussed in detail.

Dissolution of refractory elements

In this research, the choice of Mo as alloying element was based on its ability to improve the resistance to pitting in chloride environments and to crevice corrosion [14]. The presence of refractory elements in LPBF causes specific challenges, particularly in achieving complete dissolution and uniform distribution within the MP.

In the case of HEAs, the resulting microstructure strongly depends on the melting temperatures of the refractory elements and of the thermal conditions in the MP, and the wettability of the

powders. When insufficient energy densities are applied, it is more difficult for the Mo powder to be fully melted or dissolved due to its high melting point as evidenced in Fig. 2, thus leading to a reduced liquid metal volume and fluidity, promoting pore formation within MPs. The problem is even more relevant due to the formation of Mo agglomerates after the mixing process of the powders. With or without remelting, the retained Mo obstructs the flow of the metal liquid which contains other elements, leading to the formation of pores, as observed in Fig. 2b. Some partial dissolution of Mo may occur due to the transient high temperatures at the surface of the MP. In such a case, the dissolution is attributed to the convective and Marangoni flows within MPs, which promote elemental diffusion. Consequently, a comet-like morphology of Mo agglomerates is observed on the microstructure (Fig. 2a). However, the ultrafast heating and cooling rates inherent to LPBF significantly limit the time available for complete dissolution. Therefore, some Mo particles will be only partially dissolved and while the remnants are retained in agglomerates within the MPs. The application of one remelting step is not sufficient to completely dissolve high melting temperature elements such as Mo (Fig. 2b).

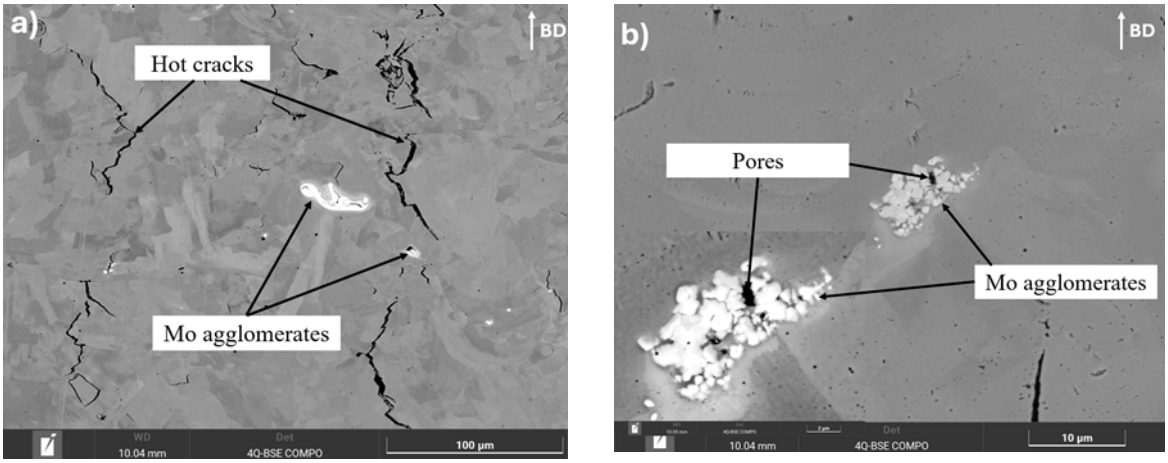

Figure 2 – SEM micrographs (a) Sample 3 (P=150W; v_s=800mm/s), (b) Sample 17 (P=175W; v_s=800mm/s, remelting).

Compositional heterogeneity of the microstructures

Chemical heterogeneity has been evidenced within all the samples, this phenomenon being extended to all the elements as shown in Fig. 3. Compositional heterogeneity is significantly influenced by medium-low energy densities and short exposure times, which result in insufficient mixing within the MP. Another factor affecting homogeneity is the blending strategy used for the powder feedstock. Manual mixing in particular, fails to ensure an uniform feedstock composition, impacting the printed parts. It has been demonstrated that irregular shape for the powders would result in poor flowability inducing in turn heterogeneous spreading in the bed. The composition heterogeneity of the elements followed the MP shape (Fig. 3 and Fig. 4) [15]. However, except for elements that did not fully dissolve in the MP, the remelting greatly improves the composition homogeneity, as observed in Fig. 4. Implementing a better mixing strategy, in addition to a remelting of each layer, is effective for decreasing the compositional heterogeneity. Shoji Aota et al. [15] suggest that remelting can be optimized by keeping the same laser and scanning parameters, while varying the hatch distance and layer thickness at the same time. Another possible strategy consists in increasing the number of remelting on each layer [16].

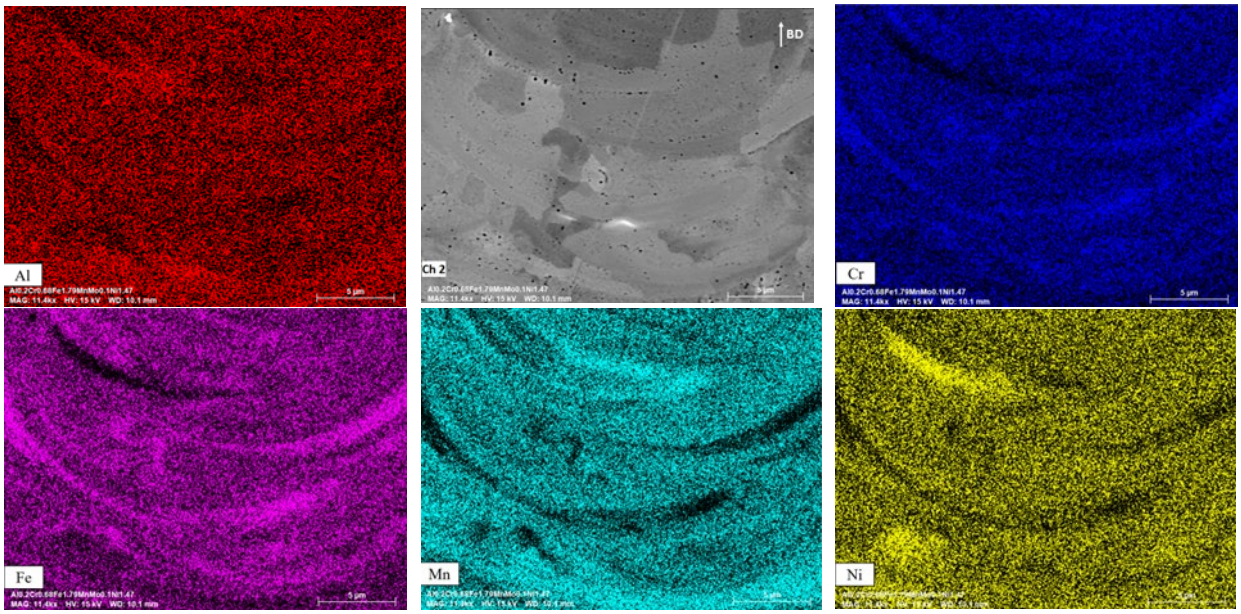

Figure 3 – EDS elemental maps for sample 3 (P=150W, v_s=800mm/s), showing fluctuations within the MP.

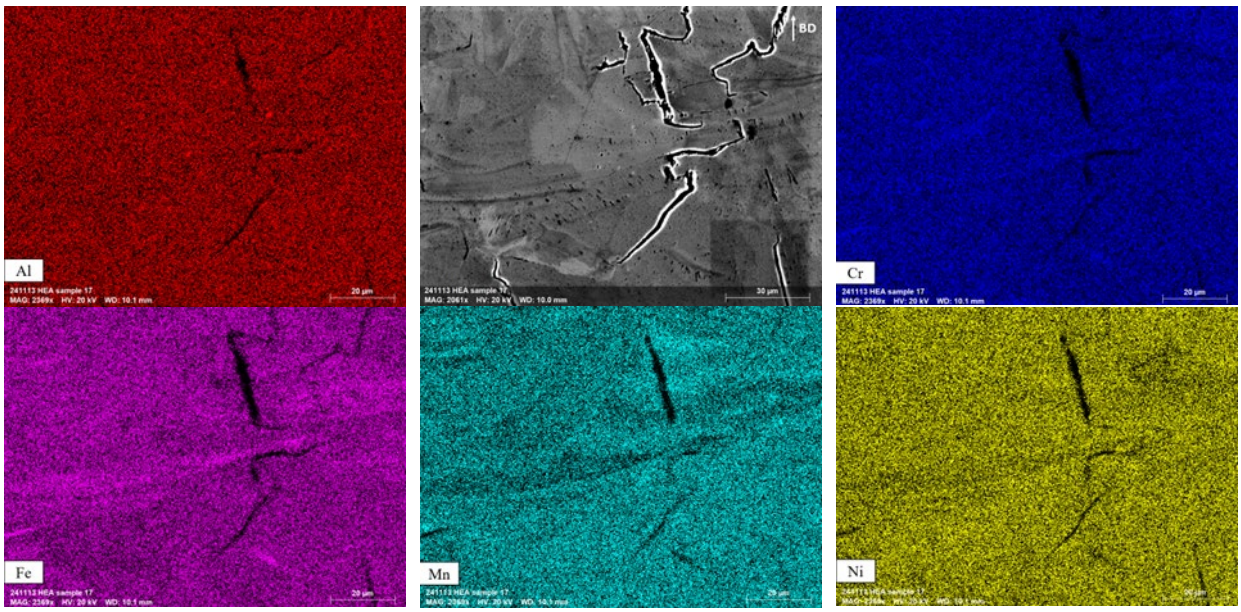

Figure 4 – EDS elemental maps for sample 17 (P=175W, v_s=800mm/s, remelting), showing crack network without element segregations.

Factors influencing hot cracks occurrence

The microstructures formed during LPBF are greatly influenced by the scanning strategy, which affects the occurrence of defects. Printing parameters can also influence the fluctuations within the MP, and thus trigger the defects formation and evolution. For instance, Marangoni flow that is driven by surface tension gradients, will lead to a high velocity on the top surface of the MP, often opposing the primary flow direction [17].

Among all the printed samples, hot cracks are consistently observed, as shown in Fig. 1. Their initiation is influenced by the complex shrinkage stress during the printing process. This phenomenon is influenced by precipitation reactions and by the formation of liquid films during solidification in relation with alloying element segregations. For instance, Tomus and al. [18] demonstrates that alloying elements like Mn and Ni play a crucial role in promoting hot cracking

during LPBF process [19,20]. As shown by the elemental distribution in Fig. 5 and Fig. 6, Si segregates at MP boundaries while promoting the formation of hot cracks in both samples. Indeed, the segregation of Si at grain boundaries strongly influences hot cracks formation by promoting the formation of detrimental phases and thus the development of intergranular hot cracks (Fig. 7). In this work, Si is prealloyed in 316L stainless steel at approximately 1 wt.%, which causes preferential segregation along grain boundaries and cracked regions. This behavior is attributed to the formation of a thin liquid film at lower temperatures, exacerbating intergranular cracking [21]. Engeli et al. [22] reported that reducing Si content in the alloy powder can significantly decrease intergranular crack density by mitigating detrimental phase formation at grain boundaries.

During the solidification, the chemical segregation at the boundaries and the distribution of elements during liquid to solid transition are governed by the relative solubility of the elements in the liquid and solid phases. This behavior is quantified by the partition coefficient, defined as the ratio of an element's equilibrium concentration in the solid phase to its concentration in the liquid phase. Agrawal et al. [23] demonstrates that the lower partition coefficients of both Mn (0.75 in FCC phase) and Si (0.5 in FCC phase) result in the segregation of these elements at the grain boundaries. This work shows that Si, with a lower partition coefficient, segregates first out of liquid phase to accumulate at the cell boundaries during the solidification process. In contrast, Mn, with relatively high partition coefficient, is more evenly distributed and retained in the solid phase during the phase transition.

Residual stresses are inherent to LPBF processing, as they are driven by the high temperature gradients between the substrate and the MP, which also lead to high solidification rates (Fig. 7). Therefore, residual stress should also be considered in the development of hot cracks. Sun et al. [24] demonstrated that residual stress induced by large grain sizes is a critical factor contributing to hot cracking in FeCoCrNi HEAs produced via LPBF. In addition, the compositional complexity of HEAs, when combined with impurities in raw materials and with the challenges associated with powder mixing strategies, further worse defect occurrence. These defects include hot cracks and chemical heterogeneities, which are difficult to mitigate without optimizing processing parameters.

As printing parameters significantly impact the residual stress field, strategies such as remelting have been proposed to mitigate this issue. However, the efficiency of the remelting steps depends on the specific printing conditions used. Literature indicates that identical scanning parameters for remelting can initially increase the residual stresses by 22-68% [25-28]. As a result, the remelting strategy adopted, consisting in one single remelting after each layer, seems to be not enough to achieve complete stress relief. In fact, the development of hot cracks might not be mitigated by the remelting.

Carter and coworkers were able to explain how the laser scan strategy can influence the cracks formation [29]. In fact, they consider the so-called island scan strategy that creates regions with high angle grain boundaries (HAGB) (>15°), which are more susceptible to crack. In contrast, a back-and-forth strategy allows a better homogeneity of the grain structures.

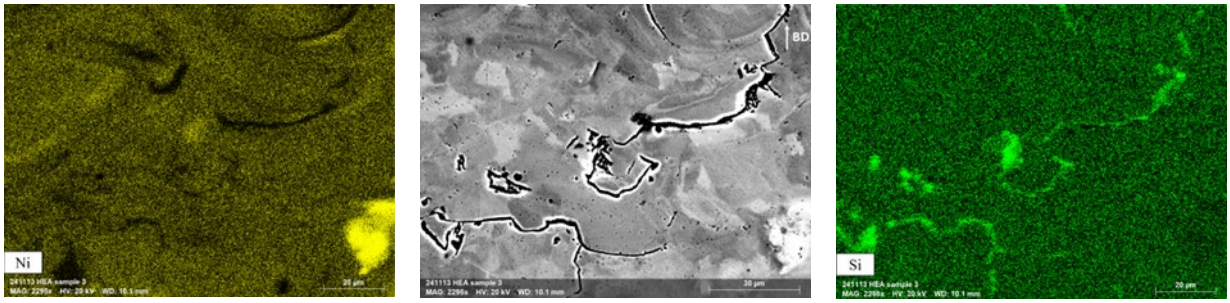

Figure 5 – EDS elemental maps for sample 3 (P=150W, v_s=800mm), showing undissolved Ni and Si segregations associated with hot cracks.

Figure 6 – EDS elemental maps for sample 17 (P=175W, v_s=800mm/s, remelting), showing undissolved Cr and Si segregations associated with hot cracks.

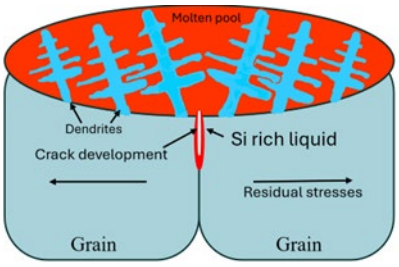

Figure 7 – Schematic diagram of the initiation of hot cracks at HAGB associated with Si segregations during solidification stage of LPBF process; inspired from Guo et al. [7].

Conclusion

Using mixture of elemental and alloy powders as feedstock for LPBF makes it easy to check for the processability of several compositions, without the need for costly atomization or other powder manufacturing processes. Nevertheless, this method faces several important issues, the most critical being the partial or non- dissolution of refractory elements such as Mo. The size of the powder can also affect the dissolution process, leading to the formation of agglomerates or comet tails, later observed inside the MP. Another challenge is the compositional heterogeneity involving a broader range of elements, which is due to the rapid cooling rates achieved during LBPF process. Moreover, elemental segregation, especially that of Si, can promote hot cracks occurrence.

To develop HEAs from powder mixtures, it is essential to address all the above issues. Reducing the particle size of refractory powders to the finest ones that ease their dissolution can be a relevant approach. Alternatively, the use of commercial powders can significantly reduce the reliance on elemental powders by combining multiple pre-alloyed powders to achieve the desired composition.

Acknowledgements

The authors acknowledge the CAREM of the ULiege for providing SEM/EDS/EBSD facilities. They also thank Sylvie Salieri for the sample preparation.

References

[1] I. Yadroitsev, I. Yadroitsava, A. du Plessis, E. MacDonald, Fundamentals of laser powder bed fusion of metals, first ed., Elsevier, 2021. https://doi.org/10.1016/B978-0-12-824090-8.00024-X

[2] A. T. Sutton, C. S. Kriewall, M. C. Leu, J.W. Newkirk, Powder characterisation techniques and effects of powder characteristics on part properties in powder-bed fusion processes, Virtual Phys. Prototyp., 12(1) (2017) 3-29. https://doi.org/10.1080/17452759.2016.1250605

[3] J. Wang, R. Zhu, Y. Liu, L. Zhang, Understanding melt pool characteristics in laser powder bed fusion: An overview of single-and multi-track melt pools for process optimization, APM, 2(4) (2023), 100137. https://doi.org/10.1016/j.apmate.2023.100137

[4] Y. Liu, Z. Liu, Y. Jiang, G. Wang, Y. Yang, L. Zhang, Gradient in microstructure and mechanical property of selective laser melted AlSi10Mg, J. Alloy. Comp.735 (2018) 1414-1421. https://doi.org/10.1016/j.jallcom.2017.11.020

[5] N.T. Aboulkhair, N.M. Everitt, I. Ashcroft, C. Tuck, Reducing pore in AlSi10Mg parts processed by selective laser melting, Addit. manuf. 1-4 (2014) 77-86. https://doi.org/10.1016/j.addma.2014.08.001

[6] H. Li, E. G. Brodie, C. Hutchinson, Predicting the chemical homogeneity in laser powder bed fusion (LPBF) of mixed powders after remelting, Addit. Manuf., 65 (2023) 103447. https://doi.org/10.1016/j.addma.2023.103447

[7] L. Guo, J. Gu, B. Gan, S. Ni, Z. Bi, Z. Wang, M. Song, Effects of elemental segregation and scanning strategy on the mechanical properties and hot cracking of a selective laser melted FeCoCrNiMn-(N, Si) high entropy alloy, J. Alloys Compd., 865 (2021) 158892. https://doi.org/10.1016/j.jallcom.2021.158892

[8] J.W. Yeh, S.K. Chen, S.J. Lin, J.Y. Gan, T.S. Chin, T.T. Shun, S.H. Tsau, S.Y. Chang, Nanostructured high-entropy alloys with multiple principal elements: novel alloy design concepts and outcomes, Adv. Eng. Mater. 6 (2004) 299-303. https://doi.org/10.1002/adem.200300567 https://doi.org/10.1002/adem.200300567

[9] B. Cantor, I.T.H. Chang, P. Knight, A.J.B. Vincent, Microstructural development in equiatomic multicomponent alloys, Mater. Sci. Eng. 375-377 (2004) 213-218. https://doi.org/10.1016/j.msea.2003.10.257

[10] Y. Zhang, T.T. Zuo, Z. Tang, M.C. Gao, K.A. Dahmen, P.K. Liaw, Z.P. Lu, Microstructures and properties of high-entropy alloys, Prog. Mater Sci. 61 (2014) 1-93. https://doi.org/10.1016/j.pmatsci.2013.10.001

[11] D.B. Miracle, O.N. Senkov, A critical review of high entropy alloys and related concepts, Acta Mater. 122 (2017) 448-511. https://doi.org/10.1016/j.actamat.2016.08.081 https://doi.org/10.1016/j.actamat.2016.08.081

[12] Y. Shi, B. Yang, P.K. Liaw, Corrosion-resistant high-entropy alloys: A review, Metals 7 (2017). https://doi.org/10.3390/met7020043 https://doi.org/10.3390/met7020043

[13] A. Giorgetti, N. Baldi, M. Palladino, F. Ceccanti, G. Arcidiacono, P. Citti, A Method to Optimize Parameters Development in L-PBF Based on Single and Multitracks Analysis: A Case Study on Inconel 718 Alloy, Metals, 13 (2) (2023). https://doi.org/10.3390/met13020306 https://doi.org/10.3390/met13020306

[14] R. Saluja, K. M. Moeed, The emphasis of phase transformations and alloying constituents on hot cracking susceptibility of type 304L and 316L stainless steel welds, Int. J. Eng. Sci. Technol., 4(5) (2012) 2206-2216.

[15] L. Shoji Aota, P. Bajaj, H. R. Zschommler Sandim, E. Aimé Jägle, Laser powder-bed fusion as an alloy development tool: Parameter selection for in-situ alloying using elemental powders, Materials, 13(18) (2020) 3922. https://doi.org/10.3390/ma13183922

[16] H. Li, E. G. Brodie, C. Hutchinson, Predicting the chemical homogeneity in laser powder bed fusion (LPBF) of mixed powders after remelting, Addit. Manuf., 65 (2023) 103447. https://doi.org/10.1016/j.addma.2023.103447

[17] T. Zhang, H. Li, S. Liu, S. Shen, H. Xie, W. Shi, G. Zhang, B. Shen, L. Chen, B. Xiao, M. Wei, Evolution of molten pool during selective laser melting of Ti-6Al-4V, J. Phys. D Appl. Phys. 59 (2019) 055302. https://doi.org/10.1088/1361-6463/aaee04

[18] D. Tomus, P.A. Rometsch, M. Heilmaier, X. Wu, Effect of minor alloying elements on crack-formation characteristics of Hastelloy-X manufactured by selective laser melting, Addit. Manuf. 16 (2017) 65-72. https://doi.org/10.1016/j.addma.2017.05.006

[19] A. Hariharan, L. Lu, J. Risse, A. Kostka, B. Gault, E.A. Jägle, D. Raabe, Misorientation-dependent solute enrichment at interfaces and its contribution to defect formation mechanisms during laser additive manufacturing of superalloys, Phys. Rev. Mater. 3 (12) (2019) 123602. https://doi.org/10.1103/PhysRevMaterials.3.123602

[20] J. Li, S.L. Shrestha, Y. Long, L. Zhijun, Z. Xintai, The formation of eutectic phases and hot cracks in one Ni-Mo-Cr superalloy, Mater. Des., 93 (2016) 324-333. https://doi.org/10.1016/j.matdes.2015.12.152

[21] L. Guo, J. Gu, B. Gan, S. Ni, Z. Bi, Z. Wang, M. Song, Effects of elemental segregation and scanning strategy on the mechanical properties and hot cracking of a selective laser melted FeCoCrNiMn-(N, Si) high entropy alloy, J. Alloys Compd., 865 (2021) 158892. https://doi.org/10.1016/j.jallcom.2021.158892

[22] R. Engeli, T. Etter, S. Hövel, and K.Wegener, Processability of different IN738LC powder batches by selective laser melting, J. Mater. Process. Technol., 229 (2016) 484. https://doi.org/10.1016/j.jmatprotec.2015.09.046

[23] P. Agrawal, S. Thapliyal, P. Agrawal, A. Dhal, R. S. Haridas, S. Gupta, R. S. Mishra, Additive manufacturing of a metastable high entropy alloy: Metastability engineered microstructural control via process variable driven elemental segregation, Mater. Sci. Eng., A 872 (2023) 144938. https://doi.org/10.1016/j.msea.2023.144938

[24] Z. Sun, X. P. Tan, M. Descoins, D. Mangelinck, S. B. Tor, C. S. Lim, Revealing hot tearing mechanism for an additively manufactured high-entropy alloy via selective laser melting, Scr. Mater., 168 (2019) 129-133. https://doi.org/10.1016/j.scriptamat.2019.04.036

[25] E. G. Brodie, E, J. Richter, T. Wegener, T. Niendorf, A. Molotnikov, Low-cycle fatigue performance of remelted laser powder bed fusion (L-PBF) biomedical Ti25Ta, Mater. Sci. Eng., A 798 (2020) 140228. https://doi.org/10.1016/j.msea.2020.140228

[26] Z. Xiao, C. Chen, Z. Hu, H. Zhu, H, X. Zeng, Effect of rescanning cycles on the characteristics of selective laser melting of Ti6Al4V, Opt. Laser Technol., 122 (2020) 105890. https://doi.org/10.1016/j.optlastec.2019.105890

[27] H. Ali, H. Ghadbeigi, K. Mumtaz, Effect of scanning strategies on residual stress and mechanical properties of Selective Laser Melted Ti6Al4V, Mater. Sci. Eng., A 712 (2018) 175-187. https://doi.org/10.1016/j.msea.2017.11.103

[28] Z. Xiong, P. Zhang, C. Tan, D. Dong, W. Ma, K. Yu, Selective laser melting and remelting of pure tungsten, Adv. Eng. Mater., 22(3) (2020) 1901352. https://doi.org/10.1002/adem.201901352

[29] L. N. Carter, C. Martin, P. J. Withers, M. M. Attallah, The influence of the laser scan strategy on grain structure and cracking behaviour in SLM powder-bed fabricated nickel superalloy, J. Alloys Compd., 615 (2014) 338-347. https://doi.org/10.1016/j.jallcom.2014.06.172